Predicting path from undulations for *C. elegans* using linear and nonlinear resistive force theory

2017 Phys. Biol. 14 025001

(http://iopscience.iop.org/1478-3975/14/2/025001)

IOP Publishing Phys. Biol. 14 (2017) 025001 https://doi.org/10.1088/1478-3975/aa5ce6

Physical Biology

OPEN ACCESS

PAPER

Predicting path from undulations for *C. elegans* using linear and nonlinear resistive force theory

Eric E Keaveny[1] and André E X Brown[2,3]

[1] Department of Mathematics, Imperial College London, London, United Kindom
[2] MRC Clinical Sciences Centre, London, United Kingdom
[3] Institute of Clinical Sciences, Imperial College London, London, United Kingdom

E-mail: e.keaveny@imperial.ac.uk **or** andre.brown@imperial.ac.uk

RECEIVED
5 September 2016

REVISED
22 December 2016

ACCEPTED FOR PUBLICATION
30 January 2017

PUBLISHED
22 March 2017

Keywords: *C. elegans*, resistive force theory, locomotion

Supplementary material for this article is available online

Abstract

A basic issue in the physics of behaviour is the mechanical relationship between an animal and its surroundings. The model nematode *C. elegans* provides an excellent platform to explore this relationship due to its anatomical simplicity. Nonetheless, the physics of nematode crawling, in which the worm undulates its body to move on a wet surface, is not completely understood and the mathematical models often used to describe this phenomenon are empirical. We confirm that linear resistive force theory, one such empirical model, is effective at predicting a worm's path from its sequence of body postures for forward crawling, reversing, and turning and for a broad range of different behavioural phenotypes observed in mutant worms. Worms recently isolated from the wild have a higher effective drag anisotropy than the laboratory-adapted strain N2 and most mutant strains. This means the wild isolates crawl with less surface slip, perhaps reflecting more efficient gaits. The drag anisotropies required to fit the observed locomotion data (70 ± 28 for the wild isolates) are significantly larger than the values measured by directly dragging worms along agar surfaces (3–10 in Rabets *et al* (2014 *Biophys. J.* **107** 1980–7)). A proposed nonlinear extension of the resistive force theory model also provides accurate predictions, but does not resolve the discrepancy between the parameters required to achieve good path prediction and the experimentally measured parameters. We confirm that linear resistive force theory provides a good effective model of worm crawling that can be used in applications such as whole-animal simulations and advanced tracking algorithms, but that the nature of the physical interaction between worms and their most commonly studied laboratory substrate remains unresolved.

Introduction

Animals move through their environment by changing the shape of their bodies. The connection between motion in space and postural change depends on the mechanical interaction between an animal and its surroundings. For example, a whale performing motions optimised for swimming does not get far if it is beached. Less extreme differences in an animal's surroundings can nonetheless be important for understanding how their gaits are related to their behavioural goals, as in the case of snakes climbing sand dunes [2] or amoebae crawling through viscous fluids [3]. These studies are especially tractable in the nematode worm *Caenorhabditis elegans* because of its small size (it can be imaged on standard microscopes) and cylindrical morphology (which simplifies analysis).

The mechanics of locomotion of *C. elegans* has been studied in aqueous media [4–7], viscous fluids [8–12], granular suspensions [13, 14], and structured environments [15–18]. *C. elegans* is also a commonly used genetic model organism with a well described nervous system, including the most complete connectome currently available. It thus offers an interesting opportunity to connect studies on the physics of behaviour with genetics and neuroscience. Most behavioural assays used in biology labs are performed with worms crawling on the surface of an agar plate, a mechanically complex medium consisting of a gel, with a water layer and air interface. A current challenge

is therefore to understand how the postural changes observed during free behaviour on an agar surface are related by mechanics to the worm's translation and rotation.

Mathematical modelling has played an important role in connecting worm body postures with its motion through the surrounding environment. For swimming, one can rely on the well-developed theories of low Reynolds number hydrodynamics that allows for the computation of the fluid flow due to undulations and subsequently, the worm's translation and rotation. In particular, due to the slenderness of the worm, one can use the approximate reduction of the full hydrodynamic problem through resistive force theory for which the force depends linearly on the velocity and the effects of the fluid are bundled into two drag coefficients—one for motion along the tangent to the worm's centreline and one for motion perpendicular to it. The drag anisotropy, ratio between the normal and tangential drag coefficients, is approximately 2 [19], and values different from unity are essential for swimming to occur. This simple model has been shown to be very effective in predicting the swimming speeds of worms and has allowed for the computation of important quantities such as the worm's elastic properties and power output [9, 12, 20, 21].

Crawling on agar, though more relevant from an experimental point of view, is more challenging. This is due to both the complicated mechanical properties of gels, as well as the nontrivial presence of the liquid film coating the gel surface. Though there have been attempts to construct crawling models from first principles that incorporate these details [22, 23], the majority of crawling models are empirical. The most prevalent empirical crawling model is an adaptation of resistive force theory. Instead of taking the drag anisotropy to be 2 as it is for swimming, it is set to a much higher value since the worm will not experience any slippage as the drag anisotropy goes to infinity. Though empirical, this model has been employed extensively and has been shown to produce worm-like locomotion and capture several aspects of the crawling kinematics [10, 24–26]. These results have been reviewed in [27] including a comparison of the results of a physics simulator using resistive force theory to analytical results for sinusoidal waveforms.

While prevalent and effective, the linear model itself is simply inferred rather than based on rational construction, be it from first principle theories or hard experimental evidence. Recently, there has been work to improve upon this and construct a resistive force model by measuring the force required to drag the worm on a gel surface both along and perpendicular to its centreline [1]. It was found that the force has a power law dependence on the velocity for motions along and perpendicular to the centreline that also depend on the percentage of agar in the gel. This reveals that the effective drag coefficients themselves depend on the velocity. The authors tested the model by holding the worm fixed as it tried to crawl and compared the force given by the model with the measured value.

In this paper, we test both the linear and nonlinear models by quantifying how well they reproduce worm paths for a number of wild-type and mutant strains. For both models, we find optimal parameter values (drag coefficients and power law exponents) by minimizing the difference between the experimental and computed paths. Our computations reveal that both the linear and nonlinear model can reproduce the worm paths accurately during sinusoidal crawling, reversals, and sharp turns and that resistive force theory is applicable across strains including uncoordinated mutants. This analysis showed that wild strains crawl with less slip than the laboratory reference strain or most mutant strains. However, to accurately reproduce the observed paths, the parameter values are not in agreement with the experimentally recorded values [1]. These results confirm that the linear model provides a good effective theory for relating worm undulations to their paths that is fast and robust but also highlight our incomplete understanding of the physics of worm crawling on the surface of agar.

Crawling models

In this section, we summarize the linear and nonlinear models and describe how they can be used to compute worm paths using undulations measured from experiments. A full description of the model is provided in the supplementary information. The MATLAB implementation of the model is available at https://github.com/aexbrown/Crawl_Model.

Linear model

In the linear model, it is assumed that the force per unit length experienced by the worm at a point s along its length (figure 1(A)) is linearly related to the velocity at which that point is moving. The drag coefficient that relates the force to the point's velocity, however, depends on whether the velocity is in the direction of the tangent to the worm, or normal to it (figure 1(B)). Accordingly, the force–velocity relationship at s can be written as

$$f_t(s) = \alpha_t U_t(s),$$

$$f_n(s) = \alpha_n U_n(s),$$

where f_t and f_n are the force per unit length in the tangent and normal directions the worm exerts on the environment, respectively, U_t and U_n are the tangential and normal components of the velocity, respectively, and α_t and α_n are the drag coefficients for tangential and normal motion, respectively.

Computing paths

We can use this model to predict the rigid body motion (translation and rotation) that results from a given shape change. The total predicted motion is then the

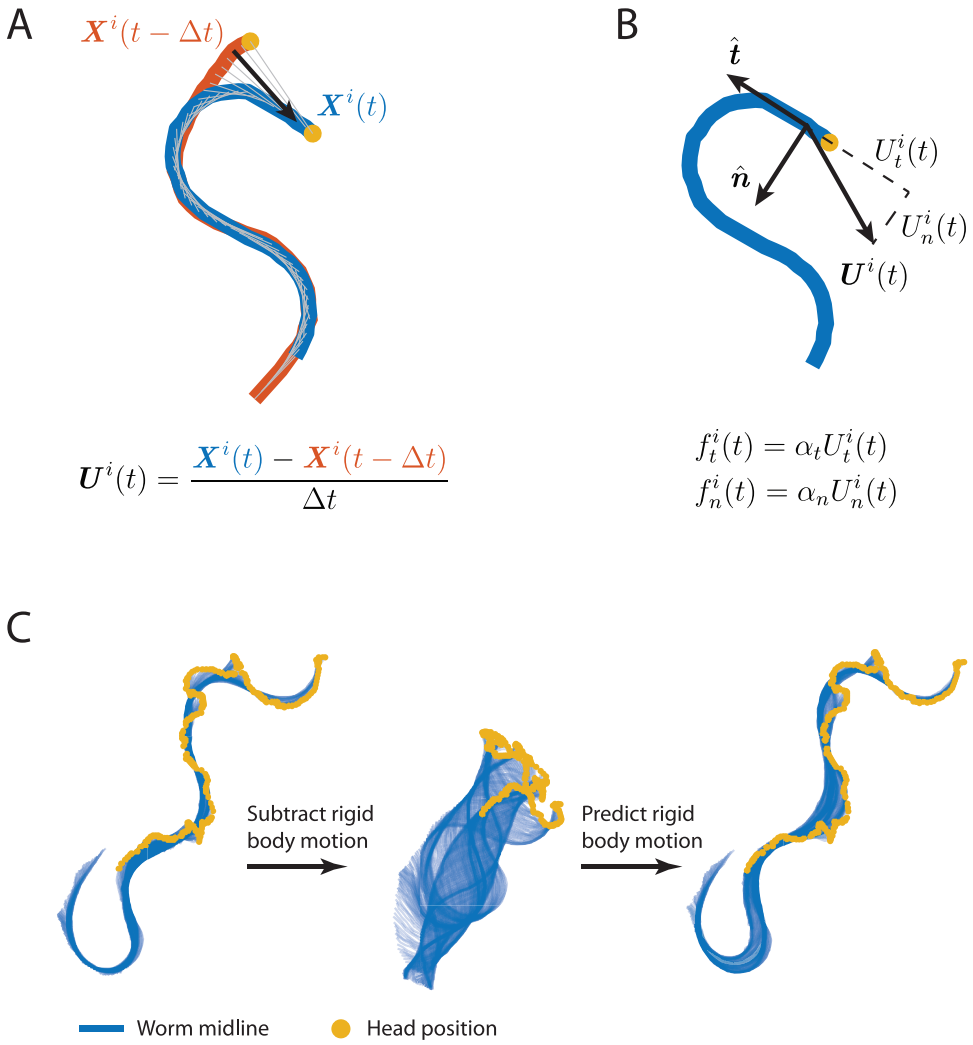

Figure 1. Model schematic and graphical outline of analysis. (A) A worm is represented by 49 points along its midline at two different times. The velocity of each point is calculated by dividing the displacement (black arrow and grey lines) by the time interval separating the two postures, Δt. (B) Each point velocity is decomposed into a tangential and normal component. The tangential and normal forces are then assumed to be proportional to these velocities, but with different constants of proportionality α_t and α_n. (C) Body undulations cause the worm to move, tracing out a sinuous path (worm head is indicated by the yellow dot). We subtract the resulting motion leaving only shape changes over time. We then use resistive force theory to predict the motion that would result from the observed shape changes.

combination of the rigid body motion with the motion of each point due to undulations. We summarize this calculation here and provide a detailed account in the supplementary information. To predict the worm paths, we first calculate the rigid body motion of the worm from the experimental measurements of the velocity, $\boldsymbol{U}(s)$, following

$$V = \frac{1}{L}\int_0^L U(s)\mathrm{d}s,$$

$$\boldsymbol{\Omega} = \frac{1}{I}\int_0^L (X(s) - X_{\mathrm{CM}}) \times U(s)\mathrm{d}s,$$

where V is the worm's translational velocity, $\boldsymbol{\Omega}$ is the angular velocity, and

$$X_{\mathrm{CM}} = \frac{1}{L}\int_0^L X(s)\ \mathrm{d}s,$$

$$I = \int_0^L (X(s) - X_{\mathrm{CM}})^2\mathrm{d}s.$$

We then subtract off the rigid body motion so what remains is only the velocity due to undulations (figure 1(C)),

$$\boldsymbol{u}(s) = \boldsymbol{U}(s) - V - \boldsymbol{\Omega} \times (X(s) - X_{\mathrm{CM}}).$$

To this, we add an unknown rigid body motion which we find by substituting our new expression for the velocity into the linear model and insisting that the total force and total torque experienced by the worm are zero,

$$F = \int_0^L f(s)\mathrm{d}s = 0\,,$$

$$\boldsymbol{\tau} = \int_0^L (X(s) - X_{\mathrm{CM}}) \times f(s)\mathrm{d}s = 0\,.$$

What results is a 3×3 system of linear equations which can be solved to find the two components of the worm's velocity and the one component of the angular velocity. The worm's path is then found by integrating the translational velocity in time (figure 1(C)).

Nonlinear model

The model introduced by Rabets *et al* [1] extends the linear model by now allowing the force per unit length to depend nonlinearly on the tangential and normal velocity components such that

$$f_t(s) = \beta_t U_t^{\gamma_t}(s),$$

$$f_n(s) = \beta_n U_n^{\gamma_n}(s),$$

where the parameters γ_t and γ_n govern the nonlinear nature of the model. When $\gamma_t = 1$ and $\gamma_n = 1$, one recovers the linear model with $\beta_t = \alpha_t$ and $\beta_n = \alpha_n$. Values of β_t, β_n, γ_t, and γ_n were found by Rabets *et al* by measuring the force required to drag the worm along an agar surface at a given speed [1].

As with the linear model, the nonlinear model can be used to predict the worm's path by following the same procedure. We subtract the rigid body motion from the worm's velocity data, such that only the motion due to undulations remains. Then, adding on an unknown rigid body motion, we substitute the velocity into the model and impose a condition of zero force and zero torque. Now, however, we must solve a system of nonlinear equations (due to the nonlinearity of the model) to find the unknown velocity and angular velocity of the worm. The details of this calculation can be found in the supplementary information.

Experimental methods

Worm tracking

The videos analysed in this paper were collected and described previously [28]. Briefly, single adult worms were placed on the centre of a 2% agar plate and allowed to habituate for 30 min. They were then recorded for 15 min and followed using a tracking stage to keep the worm in the camera's field of view. The data presented here are either from short segments of 1000 frames containing a given behaviour type (forward crawling, reversal, or turn in figures 2 and 4) or from the first 3000 frames of each video (figure 3). Each worm is segmented from the background by thresholding and skeletonised by tracing the midline between the two points of highest curvature on the outline of the segmented object (these two points correspond to the head and tail of the animal). The head is then identified using a linear classifier that considers the motion and brightness at each end. The head is typically brighter than the tail and oscillates more. The worm midline is represented by 49 equally spaced points. In addition to the laboratory strain N2, several hundred mutant strains as well as 18 wild isolates of *C. elegans* were tracked and skeletonised using the same method.

Results

We first used the linear model to predict the motion of *C. elegans* wild isolates. These are worms from the same species but isolated from different parts of the world. We reasoned that because they have not been propagated in the lab for as many generations as the reference strain N2, their gait may be more optimised for efficient locomotion. The results for several randomly chosen bouts of locomotion are shown in figure 2(A). Each segment is 1000 frames long (just over 33 s at 30 frames per second). The forward locomotion segments were selected to have a forward distance greater than 1000 μm and an average speed of greater than 250 μm s^{-1}. The reversal segments were selected to have a backwards distance greater than 1000 μm and an average absolute speed greater than 250 μm s^{-1}. The turn segments contained an omega turn detected using the method in [28] and also have an average speed greater than 250 μm s^{-1}. To move forwards, *C. elegans* propagates waves of dorso-ventral curvature along its body from head to tail. The forward locomotion segments are approximately sinusoidal and are therefore similar to the gaits most commonly considered in the literature on slender body swimming [19]. We also considered types of behaviour that may represent different locomotion regimes than forward crawling. Reversal segments are also approximately sinusoidal, but worms initially move in their recently created agar groove (as opposed to carving a groove as they move forwards). Omega turns are characterised by sharp body bends with high speeds normal to the worm body and it might be possible for the anterior part of the body to leave the existing groove during such manoeuvres.

The only free parameter in the linear model is the ratio of the normal to tangential drag coefficients. We used MATLAB's `fminsearch` to find a good value for the coefficient ratio and the resulting predicted midbody paths (gray lines) closely match the experimentally observed paths (black lines) for all of the different behaviour types. We also considered the limiting case of $\alpha_n \gg \alpha_t$ which corresponds to a no-slip regime in which the distance that the wave propagates backwards along the worm body is equal to the distance that the centre of mass moves forward over one period. The no-slip fit is reasonable, but there is a clear and consistent overshoot (red lines and figure 2(B)), indicating that during crawling on an agar surface covered with a lawn of bacteria, *C. elegans* moves with a small amount of slip. Finally, we also used the experimentally determined value of the drag coefficient ratio α_n/α_t (see figure 2 inset in Rabets *et al* [1]). The drag coefficient ratio measured in Rabets *et al* for 250 μm s^{-1} is less than 5, but we have used a value of 7 to be conservative. Using this value with the linear model results in more slip in the predicted paths resulting in a substantial undershoot (green lines and figure 2(B)). This difference could be caused by the bacterial lawn that the worms crawl through in our experiments. Rabets *et al* did their measurements directly on agar and so we also determined the optimal coefficient ratio for worms crawling without a bacterial food was 39.2 $\pm$ 11.4 (mean $\pm$ standard deviation), still larger than the

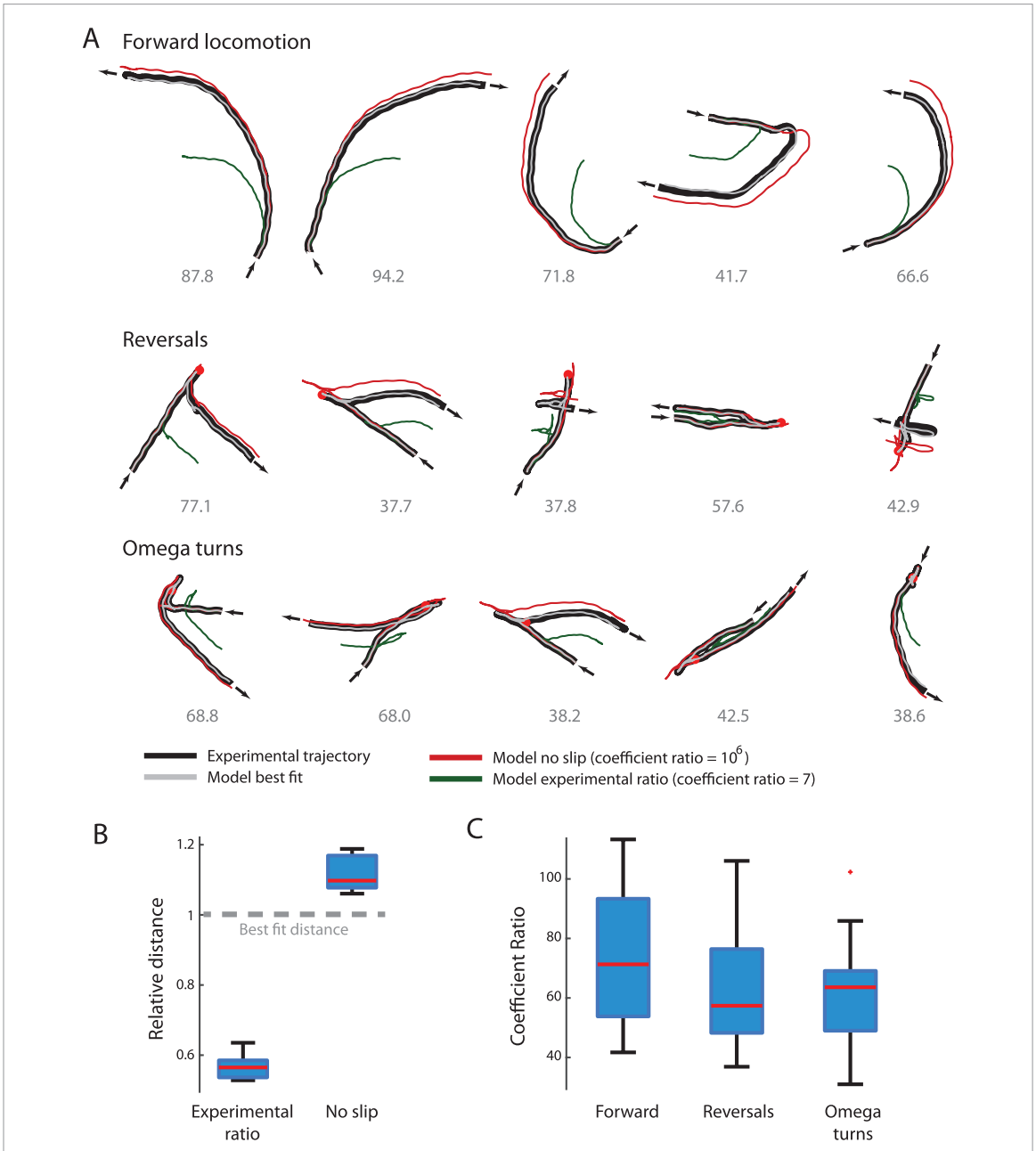

Figure 2. Linear resistive force theory accurately predicts worm paths, but not using experimentally measured drag coefficients. (A) Worm mid body paths are shown for three kinds of behaviour: forward locomotion (top), reversals (middle), and sharp turns with deep body bends (bottom). The experimental paths are shown in black overlaid with three model fits using an optimal drag coefficient ratio (grey, numbers below each trajectory give actual ratio), a high drag coefficient ratio giving a no-slip path (red), and the experimentally measured drag coefficient ratio (green). (B) Relative distance travelled for the experimentally measured ratio and the large ratio compared to the optimal ratio for 25 trajectories of each behaviour type. (C) The drag coefficient ratios determined separately for 25 trajectories of each behaviour type. None of the differences are significant with Bonferroni correction for three rank sum tests.

measured value (see also figure 3(A)). Agar dryness could also affect the observed drag coefficient ratio. We cannot rule out differences in plate preparation, but did confirm that differences in ambient humidity on experiment days do not explain the discrepancy (figure S1 (stacks.iop.org/PB/14/025001/mmedia)).

We next used the linear model to predict locomotion data for the full set of wild isolates (17 strains, 613 individuals) as well as a large set of mutants (301 strains, 8964 individuals) using fminsearch to find the optimal drag coefficient ratio. Because dividing the behaviour into subtypes (figure 2) did not have a significant effect on the best-fitting drag coefficient ratio, we simply used the first 3000 frames of data for each individual to perform the fits, which included reversals and omega turns. The wild-isolates had an optimal coefficient ratio of 70 ± 28 while the mutant coefficient ratios were comparable, but larger, with a mean of 49 ± 63 (mean $\pm$ standard deviation), consistent with the hypothesis that their locomotion is more efficient than laboratory or mutant strains (figure 3(A)). The list of worm strains ordered by median coefficient ratio is included in table S1. These values exclude cases where the coefficient ratio diverged during optimisation,

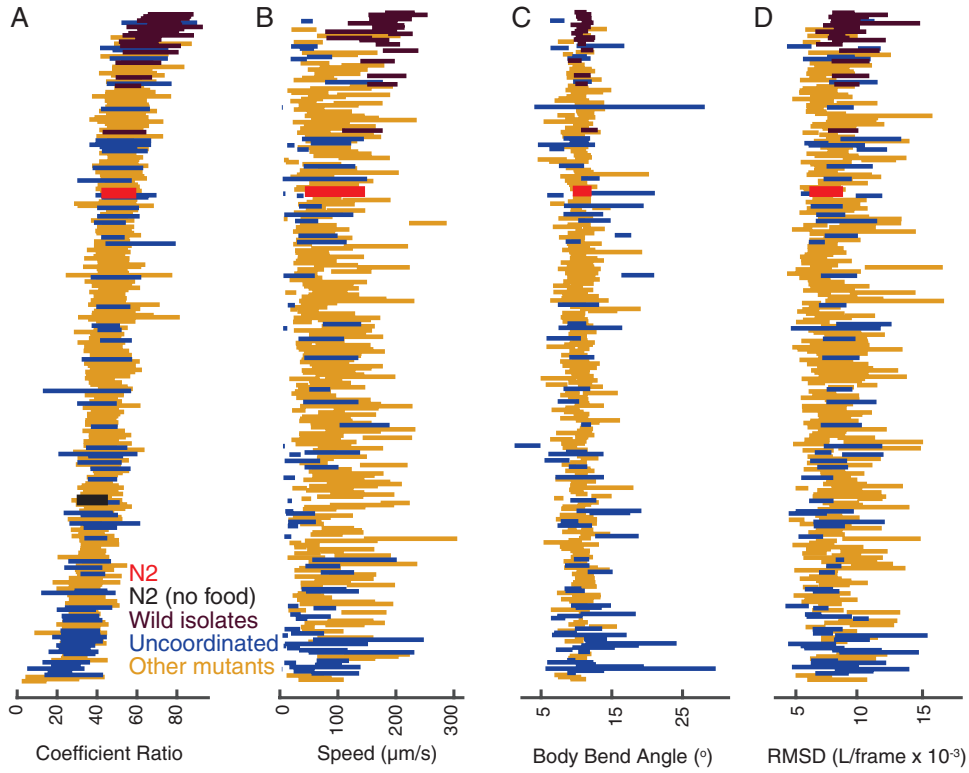

Figure 3. Wild isolates have higher drag coefficient ratios than laboratory and mutant strains. (A) The bars show the 25th–75th percentile range of drag coefficient ratio for each strain and are ordered by the median value for each strain. The colours indicate the strain. The two thicker bars are for N2 with (red) and without (black) a bacterial food lawn. (B) The speed range of each strain sorted in the same order as (A). The wild isolates are faster than the other strains, but over all there is not a strong relationship between speed and drag coefficient ratio. (C) The mid body bend angle in degrees for each strain with the same ordering as (A). (D) The root mean square deviation between the predicted and observed speed for each strain with the same ordering as (A). The RSMD is normalised for each worm by the worm length so this is the average deviation per worm length per time step.

which occurred in 1.6% of wild isolate recordings and 0.5% of mutant recordings and indicated that the no-slip condition gave the best result.

We considered two alternative explanations for the difference between the wild isolate and mutant coefficient ratio distributions. The first is that the wild isolates are known to move more persistently than the laboratory strain N2 as well as most of the mutants, and the second is that several of the mutants are known to be uncoordinated. Uncoordinated worms typically have higher body curvatures and move more slowly. It is not unreasonable that body shape could have an impact on the coefficient ratio as there is a known shape dependence in the case of low Reynolds number swimming that is apparent from the solution of the full hydrodynamics problem [29]. However, neither the speed (figure 3(B)) nor the mid-body bend angle (figure 3(C)) can explain the difference in coefficient ratio across strains. Finally, we do not see a systematic difference in fit quality across strains that might explain the difference in apparent coefficient ratio (figure 3(D)).

Although the linear model fits a wide range of paths across wild type and uncoordinated strains, the best fits are obtained with parameter ratios larger than those measured experimentally in dragging experiments [1]. We therefore also used the recently proposed nonlinear extension of the model to see if this could explain the discrepancy. The nonlinear model has four free parameters, as opposed to the linear model's single parameter. To find a fit using parameters as close as possible to the experimental parameters and for computational tractability, we took advantage of the fact that each parameter changes the effective drag coefficient ratio in a predictable manner and used a single scaling parameter φ to adjust the model parameters as follows: $\beta_t = \beta_{t_0}\varphi$, $\beta_n = \beta_{n_0}/\varphi$, $\gamma_t = \gamma_{t_0}/\varphi$, and $\gamma_n = \gamma_{n0}\varphi$. We used linear interpolation of the values reported in Rabets *et al* [1] as a function of agar concentration to estimate the values for 2% agar to be $\beta_{t_0} = 0.31$, $\beta_{n_0} = 7.1$, $\gamma_{t_0} = 0.60$, and $\gamma_{n_0} = 0.31$. We used a starting value for φ of 1.15. Even with this constraint it is possible to accurately fit worm paths using the nonlinear model (figure 4). However, like the linear model, the nonlinear model undershoots the observed paths when using experimentally determined drag coefficients and exponents.

Discussion

In this study, we tested linear and nonlinear resistive-force theory models for crawling, assessing how well they can predict worm paths given the undulation kinematics. Using an optimisation procedure, we find parameter values for the simple linear model and the more complex nonlinear model that yield paths nearly

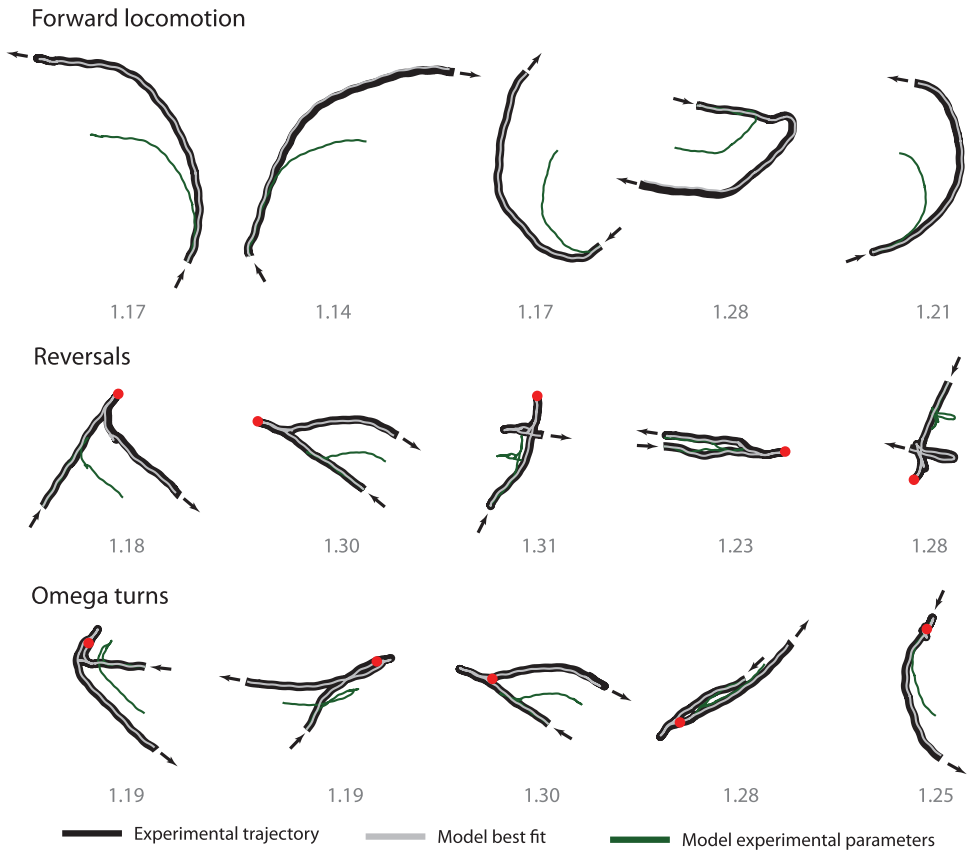

Figure 4. An extended nonlinear theory also accurately predicts worm paths, but not using experimentally measured drag coefficients. Worm mid body paths are shown for the same paths as figure 2: forward locomotion (top), reversals (middle), and sharp turns with deep body bends (bottom). The experimental paths are shown in black overlaid with two model fits; constrained best-fit coefficients (grey) and the experimentally measured coefficients (green). The number under each trajectory is φ, the fraction that each of the four nonlinear model coefficients is scaled by: $\beta_t = \beta_{t0}\varphi, \beta_n = \beta_{n0}/\varphi, \gamma_t = \gamma_{t_0}/\varphi$, and $\gamma_n = \gamma_{n0}\varphi$.

identical to those measured experimentally. For the linear model, the drag anisotropy that gives the best fit is typically high (~60), but remains finite for the vast majority of recordings, indicating that some slip yields the best results. For the nonlinear model, while we find parameter values that result in an accurate prediction of the worm's path, these parameter values do not coincide with those recently measured experimentally [1]. When we run the model with the experimentally measured values, we find a path with a similar shape, but reduced in size (figure 4). This is because the effective drag anisotropy ratio for the nonlinear model with the experimental parameter values is lower than the optimal value found for the linear model, and the nonlinear model therefore under predicts the worm's crawling speed. We note that the ability to predict the worm paths from the undulations does not give any information about the forces the worm exerts on its surrounding to produce the undulations. In the linear model, for example, the only parameter that matters is the ratio of the drag coefficients, a dimensionless quantity, rather than the values of the drag coefficients themselves. Accurately predicting the forces is essential to understand the energy the worm uses to execute different changes in posture.

Our results suggest that while we have good effective models that can accurately connect worm shape transitions to their motion, our detailed understanding of the physical interaction between the worm and the gel surface, as well as how to measure it experimentally, remains an open question. The role of the groove that worms carve in the agar as they crawl and, in particular, how it impacts the forces experienced by the worm still need to be further characterized. In the experiments performed by Rabets *et al* [1], to establish the parameter values for motion normal to the worm's centreline, the worm was dragged along the surface, thereby removing it from the groove and, perhaps, not maintaining the conditions experienced by the worm during crawling. Similarly, when testing the model, they hold the worm fixed, allowing it undulate along the surface, again, outside of any groove. Since the parameter values from these measurements did not reproduce the true worm paths, this suggests that the presence of the groove and shape of the gel surface, perhaps including a non-uniform worm depth along its length, play an important role in the how the worm propels itself.

Additionally, the models tested here are both drag based, meaning that the worm must move in order to experience any force. Such relationship would require, at the very least, a liquid layer between the worm and the gel surface. While this scenario seems to have been considered in several studies [22, 23], it may be that the worm is in contact with the surface and is exerting a

force directly on the gel. This picture would seem to be supported by the formation of the groove in the gel. Under these circumstances, the constitutive properties of the gel and how the gel deforms in response to applied forces would be directly related to how the worm moves. This would suggest that more general force relationships that incorporate yield stresses, that would allow the worm to exert a force on the surface but not move, and elasticity, as well as viscous effects, should be explored. It also suggests that variability in the worm's contact surface with the gel may also need to be considered in future models.

The ability to accurately predict worm rigid body motion from body shape changes will be useful for model-based tracking approaches [30, 31]. In these algorithms, motion in the current frame is used to predict the posture and position of the worm in the following frame. Without a quantitative connection between body shape and rigid body motion, both must be inferred independently. Independent parameter prediction increases the computational complexity of motion model tracking algorithms because the number of hypotheses to check increases exponentially in the number of degrees of freedom in the motion model. Using a mechanical model to predict the rigid body motion from the hypothesised shape changes reduces the number of independent degrees of freedom by three (x and y velocity and angular velocity). Since the posture space of *C. elegans* is already known to be relatively low-dimensional [32–34], this makes a full model of *C. elegans* locomotion quite tractable.

Finally, the tight coupling we observe between postural changes and rigid body motion shows that a direct mapping is possible between the output of the worm's nervous system, which contracts muscles, and the resulting motion in the lab frame. This supports the idea that a posture-focussed representation [35, 36] can contain essentially complete information about a worm's locomotion when it is confined to the 2D surface of an agar plate. This is a welcome simplification that facilitates computational ethology in *C. elegans* compared to many other animals where their base of support can be a critical component of their behaviour [37] that is not directly measurable with 2D imaging.

Acknowledgments

We would like to acknowledge Tianjiao Liu for preliminary work on path prediction and Kezhi Li for careful reading of the manuscript. This work was partially funded by the Medical Research Council through grant MC-A658-5TY30 to AEXB. Some strains were provided by the CGC, which is funded by NIH Office of Research Infrastructure Programs (P40 OD010440).

References

[1] Rabets Y, Backholm M, Dalnoki-Veress K and Ryu W S 2014 Direct measurements of drag forces in *C. elegans* crawling locomotion *Biophys. J.* **107** 1980–7
[2] Astley H C, Gong C, Dai J, Travers M, Serrano M M, Vela P A, Choset H, Mendelson J R, Hu D L and Goldman D I 2015 Modulation of orthogonal body waves enables high maneuverability in sidewinding locomotion *Proc. Natl Acad. Sci. USA* **112** 6200–5
[3] Barry N P and Bretscher M S 2010 Dictyostelium amoebae and neutrophils can swim *Proc. Natl Acad. Sci. USA* **107** 11376–80
[4] Gray J and Lissmann H W 1964 The locomotion of nematodes *J. Exp. Biol.* **41** 135–54
[5] Pierce-Shimomura J T, Chen B L, Mun J J, Ho R, Sarkis R and McIntire S L 2008 Genetic analysis of crawling and swimming locomotory patterns in *C. elegans Proc. Natl Acad. Sci. USA* **105** 20982–7
[6] Sznitman J, Shen X, Sznitman R and Arratia P E 2010 Propulsive force measurements and flow behavior of undulatory swimmers at low Reynolds number *Phys. Fluids* **22** 121901
[7] Restif C, Ibáñez-Ventoso C, Vora M M, Guo S, Metaxas D and Driscoll M 2014 CeleST: computer vision software for quantitative analysis of *C. elegans* swim behavior reveals novel features of locomotion *PLoS Comput. Biol.* **10** e1003702
[8] Korta J, Clark D A, Gabel C V, Mahadevan L and Samuel A D T 2007 Mechanosensation and mechanical load modulate the locomotory gait of swimming *C. elegans J. Exp. Biol.* **210** 2383–9
[9] Fang-Yen C, Wyart M, Xie J, Kawai R, Kodger T, Chen S, Wen Q and Samuel A D T 2010 Biomechanical analysis of gait adaptation in the nematode *Caenorhabditis elegans Proc. Natl Acad. Sci. USA* **107** 20323–8
[10] Berri S, Boyle J H, Tassieri M, Hope I A and Cohen N 2009 Forward locomotion of the nematode *C. elegans* is achieved through modulation of a single gait *HFSP J.* **3** 186–93
[11] Sznitman J, Shen X, Purohit P K and Arratia P E 2010 The effects of fluid viscosity on the kinematics and material properties of *C. elegans* swimming at low Reynolds number *Exp. Mech.* **50** 1303–11
[12] Backholm M, Kasper A K S, Schulman R D, Ryu W S and Dalnoki-Veress K 2015 The effects of viscosity on the undulatory swimming dynamics of *C. elegans Phys. Fluids* **27** 91901
[13] Juarez G, Lu K, Sznitman J and Arratia P E 2010 Motility of small nematodes in wet granular media *Europhys. Lett.* **92** 44002
[14] Jung S 2010 *Caenorhabditis elegans* swimming in a saturated particulate system *Phys. Fluids* **22** 31903
[15] Majmudar T, Keaveny E E, Zhang J and Shelley M J 2012 Experiments and theory of undulatory locomotion in a simple structured medium *J. R. Soc. Interface* **9** 1809–23
[16] Park S, Hwang H, Nam S-W, Martinez F, Austin R H and Ryu W S 2008 Enhanced *Caenorhabditis elegans* locomotion in a structured microfluidic environment *PLoS One* **3** e2550
[17] Lockery S R, Lawton K J, Doll J C, Faumont S, Coulthard S M, Thiele T R, Chronis N, McCormick K E, Goodman M B and Pruitt B L 2008 Artificial dirt: microfluidic substrates for nematode neurobiology and behavior *J. Neurophysiol.* **99** 3136–43
[18] Ghanbari A, Nock V, Johari S, Blaikie R, Chen X and Wang W 2012 A micropillar-based on-chip system for continuous force measurement of *C. elegans J. Micromech. Microeng.* **22** 95009
[19] Childress S 1981 *Mechanics of Swimming and Flying* (Cambridge: Cambridge University Press)
[20] Sznitman J, Purohit P K, Krajacic P, Lamitina T and Arratia P E 2010 Material properties of *Caenorhabditis elegans* swimming at low Reynolds number *Biophys. J.* **98** 617–26

[21] Krajacic P, Shen X, Purohit P K, Arratia P and Lamitina T 2012 Biomechanical profiling of *Caenorhabditis elegans* motility *Genetics* **191** 1015–21
[22] Shen X N, Sznitman J, Krajacic P, Lamitina T and Arratia P E 2012 Undulatory locomotion of *Caenorhabditis elegans* on wet surfaces *Biophys. J.* **102** 2772–81
[23] Sauvage P, Argentina M, Drappier J, Senden T, Siméon J and Di Meglio J-M 2011 An elasto-hydrodynamical model of friction for the locomotion of *Caenorhabditis elegans J. Biomech.* **44** 1117–22
[24] Niebur E and Erdös P 1991 Theory of the locomotion of nematodes *Biophys. J.* **60** 1132–46
[25] Karbowski J, Cronin C J, Seah A, Mendel J E, Cleary D and Sternberg P W 2006 Conservation rules, their breakdown, and optimality in *Caenorhabditis sinusoidal* locomotion *J. Theor. Biol.* **242** 652–69
[26] Boyle J H, Berri S, Tassieri M, Hope I A and Cohen N 2011 Gait modulation in *C. Elegans*: it's not a choice, it's a reflex! *Front. Behav. Neurosci.* **5** 10
[27] Cohen N and Boyle J H 2010 Swimming at low Reynolds number: a beginners guide to undulatory locomotion *Contemp. Phys.* **51** 103–23
[28] Yemini E, Jucikas T, Grundy L J, Brown A E X and Schafer W R 2013 A database of *Caenorhabditis elegans* behavioral phenotypes *Nat. Methods* **10** 877–9
[29] Lighthill J 1976 Flagellar hydrodynamics *SIAM Rev.* **18** 161–230
[30] Fontaine E, Burdick J and Barr A 2006 *Automated Tracking of Multiple C. Elegans* (Piscataway, NJ: IEEE) pp 3716–9
[31] Roussel N, Morton C A, Finger F P and Roysam B 2007 A computational model for *C. elegans* locomotory behavior: application to multiworm tracking *IEEE Trans. Biomed. Eng.* **54** 1786–97
[32] Stephens G J, Johnson-Kerner B, Bialek W and Ryu W S 2008 Dimensionality and dynamics in the behavior of *C. elegans PLoS Comput. Biol.* **4** e1000028
[33] Brown A E X, Yemini E I, Grundy L J, Jucikas T and Schafer W R 2013 A dictionary of behavioral motifs reveals clusters of genes affecting *Caenorhabditis elegans* locomotion *Proc. Natl Acad. Sci. USA* **110** 791–6
[34] Gyenes B and Brown A E X 2016 Deriving shape-based features for *C. elegans* locomotion using dimensionality reduction methods *Front. Behav. Neurosci.* **10** 159
[35] Schwarz R F, Branicky R, Grundy L J, Schafer W R and Brown A E X 2015 Changes in postural syntax characterize sensory modulation and natural variation of *C. elegans* locomotion *PLoS Comput. Biol.* **11** e1004322
[36] Gomez-Marin A, Stephens G J and Brown A E X 2016 Hierarchical compression of *Caenorhabditis elegans* locomotion reveals phenotypic differences in the organization of behaviour *J. R. Soc. Interface* **13** 20160466
[37] Golani I 1992 A mobility gradient in the organization of vertebrate movement: The perception of movement through symbolic language *Behav. Brain Sci.* **15** 249–66